Exp Fluids
DOI 10.1007/s00348-007-0339-6

RESEARCH ARTICLE

Water-walking devices

David L. Hu · Manu Prakash · Brian Chan · John W. M. Bush

Received: 7 February 2007 / Revised: 9 May 2007 / Accepted: 1 June 2007

Abstract We report recent efforts in the design and construction of water-walking machines inspired by insects and spiders. The fundamental physical constraints on the size, proportion and dynamics of natural water-walkers are enumerated and used as design criteria for analogous mechanical devices. We report devices capable of rowing along the surface, leaping off the surface and climbing menisci by deforming the free surface. The most critical design constraint is that the devices be lightweight and non-wetting. Microscale manufacturing techniques and new man-made materials such as hydrophobic coatings and thermally actuated wires are implemented. Using high-speed cinematography and flow visualization, we compare the functionality and dynamics of our devices with those of their natural counterparts.

Electronic supplementary material The online version of this article (doi:10.1007/s00348-007-0339-6) contains supplementary material, which is available to authorized users.

D. L. Hu · J. W. M. Bush (✉)
Department of Mathematics,
Massachusetts Institute of Technology,
Cambridge, MA, USA
e-mail: bush@math.mit.edu

Present Address:
D. L. Hu
The Courant Institute, New York University,
New York, NY, USA

M. Prakash
Center for Bits and Atoms,
Massachusetts Institute of Technology,
Cambridge, MA, USA

B. Chan
Department of Mechanical Engineering,
Massachusetts Institute of Technology,
Cambridge, MA, USA

1 Introduction

Nature has much to teach us about innovative, optimal and versatile designs. Since its inception, biomimetics has grown increasingly interdisciplinary, merging biology with nanotechnology, engineering and applied mathematics. The interface of these fields has led to the invention of diverse devices and materials, from gecko-inspired tape (Geim et al. 2003) to a dolphin-skin-inspired torpedo shell (Fish 2006). Biomimetic robots are now being built to emulate birds (Dickinson et al. 1999), fish (Triantafyllou et al. 2000) and turtles (Long et al. 2006); some recent developments are reported in this issue. In this paper, we present a few relatively modest devices capable of a form of locomotion that has been largely neglected in biomimetics: walking on water.

Nearly three centuries ago, the biologist Ray (1710) reported with amazement the ability of certain insects (*Mesovelia*) to run from land across the water surface without slowing. Recently, progress has been made towards the classification of the various means of walking on water (Bush and Hu 2006) and the development of the first water-walking devices based on nature's designs (Hu et al. 2003; Suhr et al. 2005; Song et al. 2006; Floyd et al. 2006). Unlike devices inspired by swimming and flying creatures, water-walking devices must contend with the additional challenge of staying atop the water surface. We identify in this paper a minimum number of design principles relevant for water-walkers and apply these principles in the construction of a number of water-walking devices.

We begin with a review of previously built biomimetic water-walking devices. Water-walkers can be classified as large or small according to the magnitude of the Baudoin number $Ba = \frac{Mg}{\sigma P}$, where Mg is the creature's weight, σP its maximum supporting surface tension force, P its contact perimeter and $\sigma = 70$ dynes/cm the surface tension of water (Baudoin 1955; Bush and Hu 2006). Large water-walkers ($Ba > 1$) cannot rely on surface tension for static support. Certain lizards and shorebirds can dash across water by slapping the surface with their feet, thereby supporting their weight with a combination of fluid inertia, buoyancy and added mass forces (Glasheen and McMahon 1996b). A machine capable of running on water in a manner similar to the basilisk lizard is being developed by Floyd et al. (2006). However, this feat is beyond the capabilities of humans due to their inherent power limitations (Glasheen and McMahon 1996a). Man may only walk on water using flotation devices, which are generally plodding and cumbersome. The first such device resembled floating cross-country skis and was implemented by fifteenth century ninja (Heishichiro et al. 1966); a similar design was envisioned by Leonardo da Vinci (1478–1518).

Small water-walkers ($Ba < 1$) can reside at rest on the water surface, supported by surface tension. Their means of locomotion have inspired the devices reported here. The most common water-walking insect is the water strider, which propels itself by rowing with its long middle legs. The water strider has a key adaptation common among water-walking insects: its legs are covered with a dense mat of hair that renders them effectively non-wetting (Andersen 1976; Gao and Jiang 2004; Bush et al. 2007). The first biomimetic water strider leg was designed by Shi et al. (2005) by means of electrochemical deposition of gold aggregates. The first mechanical water strider was reported by Hu et al. (2003) and is detailed in Sect. 3. Recently, Suhr et al. (2005), Song et al. (2006) constructed a new generation of biomimetic water striders capable of turning and remote-controlled motion on the water surface. A thermally actuated mechanical water strider is reported in Sect. 3.

In addition to propelling themselves laterally along the free surface, many water-walking insects and spiders can leap vertically. The dynamics of leaping off the free surface was first studied by Suter and Gruenwald (2000) in the context of the fisher spider. Theoretical work on jumping off the free surface was reported by Li et al. (2005), who considered the dynamics of a floating spring-mass system and examined the dynamical importance of compression length and spring stiffness. In Sect. 4, we describe the first mechanical device capable of leaping off the water surface.

It would seem obvious that an insect must move its legs in order to propel itself. However, in the presence of a meniscus, some water-walking insects can move simply by deforming the free surface: by maintaining certain fixed postures, they can ascend fluid menisci in a quasi-static manner (Hu and Bush 2005). Baudoin (1955) first observed this type of motion in *Dryops*, which ascends a fluid meniscus by arching its back. He showed that bent metal strips do likewise if he bent the strips so that they have the same curvature as the meniscus. Floating hexagons also propel themselves quasi-statically into a tessellation, as shown by Whitesides and Grzybowski (2002). In Sect. 5 we present a simple design for a mechanized meniscus climber.

In Sect. 2, we enumerate the physical constraints that guided us in designing our devices. Thereafter, we report the designs of our mechanical water-walkers and accompanying descriptions of the insects that inspired them. In Sect. 3, we present a mechanical rower based on the water strider *Gerris*; in Sect. 4 a leaper based on the springtail *Podura aquatica*; and in Sect. 5 a mechanical meniscus climber based on the beetle larva *Pyrrhalta*.

2 Design principles

We have based the design of our small water-walking devices on the following fundamental principles. First and foremost, the device must be hydrophobic in order to prevent its penetrating and adhering to the free surface (Bush et al. 2007). Second, it must be sufficiently lightweight to reside at rest on the free surface. Since water-walking insects are more dense than water, they cannot rely exclusively on buoyancy forces for weight support; instead, their weight Mg must be supported by curvature forces: $Ba = \frac{Mg}{\sigma P} < 1$. Thirdly, we require that the driving leg never be completely wetted during its stroke. In nature, this is accomplished by a dense mat of hairs that preclude the intrusion of water onto the driving leg; contact with the water is limited to the hair tips. In our devices, complete wetting is discouraged by the use of water-repellent materials. Finally, where possible, the devices have been designed to resemble their natural counterparts, having the same number of limbs and body proportions.

These design constraints for the mechanical water-walkers may be satisfied by maintaining dynamic similarity with their natural counterparts. The driving leg can be modeled as a cylinder of radius w and length L striking the free surface with a peak speed U, rowing frequency f, and applied force per unit length F. Buckingham's Theorem (McMahon and Bonner 1985) indicates that this reduced insect-fluid system for a given impact geometry is uniquely prescribed in terms of six dimensionless groups: the Reynolds number $Re = Uw/\nu$, Bond number $Bo = \rho g w^2/\sigma$, Weber number $We = \rho U^2 w/\sigma$ and Strouhal number $St = (wf)/U$, aspect ratio $\lambda = w/L$ and Andersen number

F/σ, where v and ρ are the viscosity and density of water and where F. These dimensionless groups relate the relative magnitudes of the propulsive forces used by the water-walker (Bush and Hu 2006). All designs were aimed at achieving dynamic similarity between the mechanical device and its natural counterpart, and so matching these dimensionless groups.

3 Rowing

The biomimetic device in Fig. 1 was inspired by the most common of water-walking insects, the water strider. The water strider's typical gait consists of a sculling motion of its middle legs against the free surface; this gait involves two phases. The first is a propulsive phase in which it drives its central pair of legs backwards against the free surface (Andersen 1976; Hu et al. 2003). The next is a recovery phase in which the strider recocks its legs for the next stroke as it glides to a stop. By varying the strength and angle of the driving stroke, the water strider either glides across the surface or leaps vertically.

Robostrider (R1), originally reported in Hu et al.(2003), is a self-contained device that rows without breaking through the water surface. The body plan is detailed in Fig. 1. Measuring 13 cm from leg tip-to-tip, it is comparable in size to the world's largest water strider, *Gigantometra gigas* (Tseng and Rowe 1999). Despite its size, its aluminum frame makes it sufficiently lightweight (0.35 g) to be supported by surface tension, as indicated by its Baudoin number in Table 2. Like its natural counterpart, R1 sits on the water surface on its front and back pairs of legs. The legs are cut from hydrophobic stainless steel wire (0.2 mm gauge), and the body from aluminum sheet (thickness 0.13) cut from a beverage can.

R1 is driven by its middle legs that are actuated by the lightweight pulley apparatus detailed in the inset of Fig. 1. The middle legs are attached to the axis of a nylon pulley (radius $R_1 = 0.09$ cm). An elastic band (9 cm length, elastic modulus $k = 3{,}100$ dynes per unit strain) is anchored on one end to the pulley, on the other end to the rear of the body. The device is loaded by winding the pulley; when released, the tension of the elastic band rotates the pulley, driving the rowing leg tips in a circular motion of radius $R_2 = 1$ cm. It is critical that the leg tips do not penetrate the surface during the stroke; subtle tuning of the orientation of the driving legs is thus generally required. The total force applied by R1's legs can be readily calculated for this simple system: using a torque balance on the driving leg, the total force may be written $2F = F_e R_1/R_2$ where the force F_e provided by the elastic band is given by Hooke's law, $F_e = k\varepsilon$ where k is the elastic modulus and ε the maximum strain. A rubber band of elastic modulus 3,100 dynes per unit strain and maximum strain 1.5 was chosen that produced a force per length of the driving legs of 30 dynes/cm. Since this force per unit length is less than 2σ, curvature forces adequately resist the submergence of the driving leg.

The dynamics of R1 was studied using high-speed video at 500 fps (Fig. 2). Its dynamics are characterized in Tables 1 and 2. The maximum distance travelled by R1 with a fully wound pulley was 20 cm, or five leg strokes (Fig. 2c). Flow visualization using thymol blue showed that R1 generates a wake containing vortices similar in form to, but less coherent than, those generated by water striders (Fig. 2b; Hu et al. 2003). Generally, the leg tips did

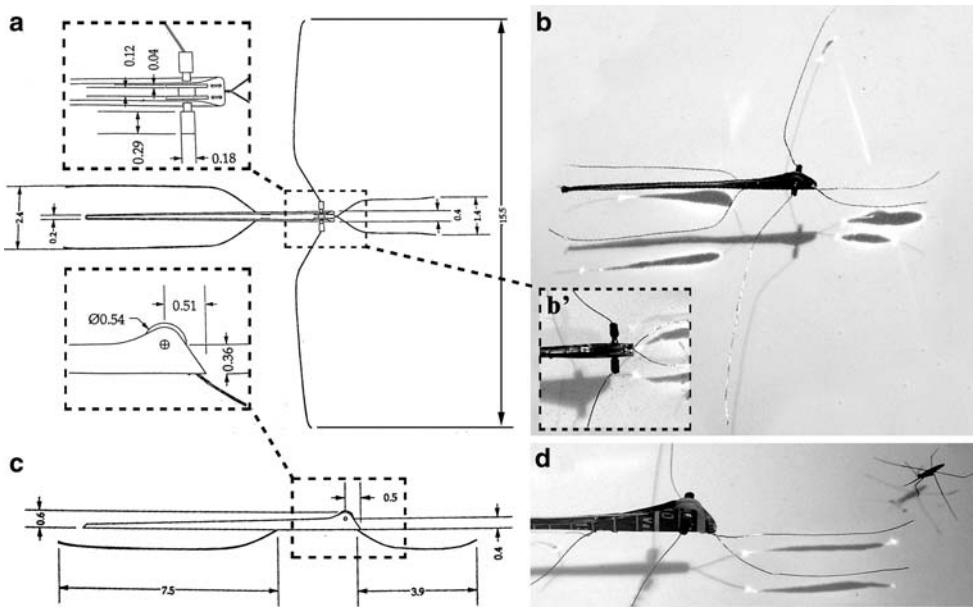

Fig. 1 Schematic diagrams of Robostrider 1 (R1) in plan (**a–b**) and side views (**c–d**). Insets detail the pulley and elastic string driving mechanism. At rest, R1 sits on the free surface on its pairs of front and hind legs. During locomotion, an elastic thread wrapped around the pulley rotates the central driving legs in a circular rowing motion that propels the device forward. All units in cm

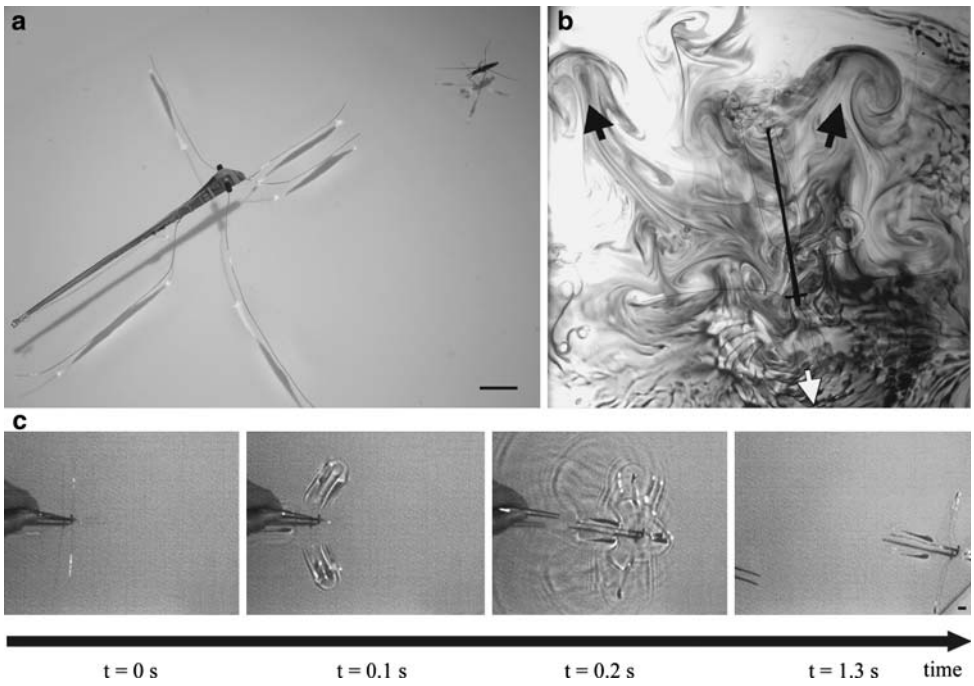

Fig. 2 **a** R1 facing its natural counterpart, *Gerris remigis*. R1 is 9 cm long and is powered by an elastic band running down its length. **b** R1 generates dipolar vortices in its wake, as visualized using thymol blue. The direction of R1 and its vortices are indicated by the *white* and *black arrows*, respectively. **c** High-speed video frames of R1's motion during five rowing strokes. R1 is released by hand (at *left* in **c**). The device is lit from above; consequently, shadows are cast by surface deformations associated with static menisci (**a**) or waves generated by the driving stroke (**c**). *Scale bars* 1 cm

Table 1 Physical parameters describing the geometry and dynamics of the water strider and its mechanical counterparts (R1 and R2)

	Leg radius w (cm)	Leg length L (cm)	Body weight Mg (dyn)	Leg speed U (cm/s)	Leg frequency f (1/s)	Leg perimeter P (cm)	Applied force/unit length F (dyn/cm)
Strider	0.006	0.6	4.5	27	100	2.2	60
R1	0.009	4.3	350	20	60	50	30
R2	0.025	1.2	70	5	5	10	20

Table 2 Dimensionless groups characterizing the geometry and dynamics of the water strider and its mechanical counterparts (R1 and R2)

	Leg aspect ratio $\lambda = \frac{w}{L}$	Reynolds $Re = \frac{Uw}{\nu}$	Bond $Bo = \frac{\rho g w^2}{\sigma}$	Weber $We = \frac{\rho U^2 w}{\sigma}$	Strouhal $St = \frac{wf}{U}$	Andersen $An = \frac{F}{\sigma}$	Baudoin $Ba = \frac{\mathrm{Mg}}{\sigma P}$
Strider	0.01	16	5×10^{-4}	6×10^{-2}	2×10^{-2}	0.4	0.03
R1	0.002	16	1×10^{-3}	4×10^{-2}	3×10^{-2}	0.7	0.08
R2	0.02	12	9×10^{-3}	9×10^{-3}	2×10^{-2}	0.3	0.12

not penetrate the water surface despite speeds in excess of 20 cm/s. The greatest challenge in deploying R1 was maintaining its hydrophobicity. While water striders are able to dry their legs by grooming, R1 had to be dried by hand between runs in order to maintain its water-repellency and so prevent its sinking.

For locomotion of longer duration, we built another mechanical water strider, Robostrider 2 (R2) that is closer in size and weight to its natural counterpart. The body of R2 was laser micro-machined from a single piece of steel shim stock (thickness 0.04 cm), shown in Fig. 3. The legs of the machine were coated with non-wetting Teflon (AF16 Dupont), which provided a static contact angle θ of 104°, comparable to the value reported on insect cuticle by Holdgate (1955). We note, however, that the surface roughness is qualitatively different on the legs of R2 and its natural counterpart, the latter being characterized by a piliferous layer that maintains an air layer between the water and the bulk of the leg surface (Bush et al. 2007).

R2's driving legs are composed of bi-layered cantilevers, consisting of a thin and thick segments, as shown in the inset of Fig. 3 (Luo et al. 2005). When a voltage (10 V) is applied to the leg, the thin part of the cantilever heats up faster and elongates more than the thick part, which bends the cantilever 2 mm and drives the leg in a sculling motion. These actuators are seamlessly integrated into the body of

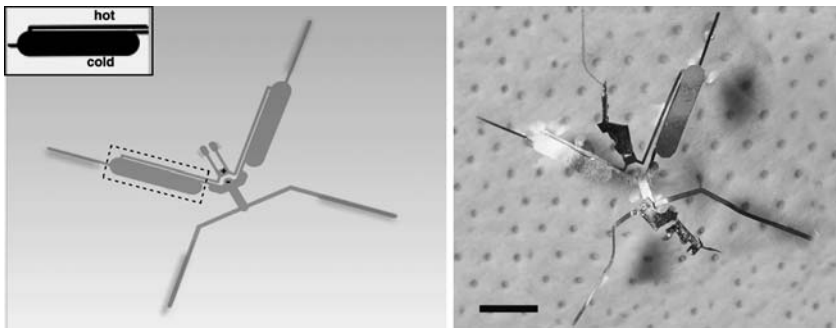

Fig. 3 R2 has built-in heat actuators to power the driving stroke. The *left inset* shows the details of the leg, which consists of a bi-layered cantilever. When a voltage is applied to the leg, the thinner layer of the cantilever heats up faster and lengthens more than the thicker layer, causing the cantilever to bend and R2 to stroke. Under an applied voltage of 10 V, the maximum deflection of the leg tip is 2 mm. *Scale bar* 1 cm

R2 in order to reduce its total weight to 0.07 g. Also, to reduce the weight, the power source for the thermal actuators was wired to an external voltage source.

The dynamics of R2, and the pros and cons over its predecessor, were assessed using high speed video of its motion. While the size of R2 is comparable to its natural counterpart, its slow body speed (2 mm/s) is two orders of magnitude lower. Unlike its predecessor, R2 has an external power supply that permits it to travel indefinitely. While R1 was hand-made, R2 was manufactured by computer-controlled machining (a similar technique as used in Fearing et al. 2000), allowing it to be made much smaller. Moreover, this production method lends itself easily to mass production and upgradability. Currently, R2's legs are wired in parallel, which makes it capable of only straight-line motion. However, by wiring each of the legs independently, R2 may be easily given turning capabilities. One disadvantage of R2's design is that there is an inherent upper limit to its maximum speed. Excessively high applied voltage results in the formation of bubbles at the leg's contact line. Insulating surface coatings would allow for the application of higher driving voltages and so higher speeds.

4 Leaping

Many water-walkers leap from the free surface (Suter and Gruenwald 2000; Suter 2003), but it was the impressive leaping ability of *Podura aquatica* that inspired our mechanical leaper. The 1 mm long *Podura* ratchets a spring-loaded forked tail called a furca at its underbelly, as shown in Fig. 4. To leap, it releases the furca which strikes the free surface, catapulting it upwards to heights of 2 cm, or 20 body lengths. High-speed video indicates that the furca is ratcheted for 100 ms and then released over a time scale of 1 ms. It is noteworthy that this is the fastest movement reported for any water-walker.

Owing to difficulties in designing on a small scale, Roboleaper (RL) was constructed to be ten times larger than its natural counterpart (Fig. 5). It consists of a curved leaf spring with a latch that is engaged by hand and released by heating with a soldering iron (Fig. 6). As the ends of the spring are released, its leaves strike the surface, catapulting RL upward. Its mass m of 4 mg makes it sufficiently light that it may be supported by surface tension; its Teflon AF16 (Dupont) coating renders it sufficiently non-wetting to detach from the free surface. We note that hydrophobicity is a critical requirement for the leaper: uncoated leaf springs were unable to detach from the free surface.

In order to leap to achieve an initial speed v, the bending energy initially stored in the spring must exceed the leaper's initial kinetic energy $\frac{1}{2}mv^2$:

$$\frac{EIL}{2R^2} > \frac{1}{2}mv^2 \tag{1}$$

where E is the the Young's modulus, I the area moment of inertia, L the length of the spring and R the radius of the circular arc (Landau and Lifshitz 1986). We were able to generate leaps of height $H \approx 10$ cm using a Kapton HN Polyimide (Dupont) sheet with density 1.4 g/cm^3, Young's modulus 2.5×10^9 dynes/cm^2, length L, width w, and thickness t listed in Table 3. The bending energy for these values is approximately 130–200 dynes cm and the initial kinetic energy only 80 dynes cm. The difference in these energies reflects the transfer of kinetic energy (KE) to the underlying fluid, the generation of surface energy (SE) in deforming the free surface, losses due to viscous dissipation (Φ), and the work done in detaching from the free surface (W_D). Rough estimates suggest characteristic values of KE of 50 dynes cm, SE and W_D less than 30 dynes cm and negligible viscous dissipation. The dominance of kinetic over surface energies is also reflected in the rupture of the interface following take-off. Note that if

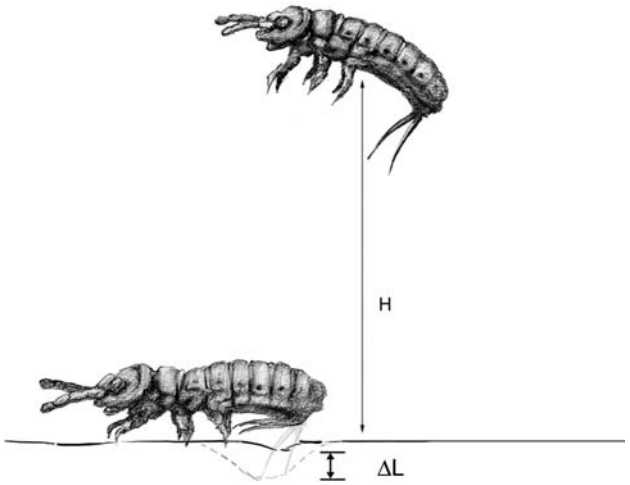

Fig. 4 The water-walking springtail *Podura aquatica* (length 2 mm) drawn from photographs. The spring-loaded forked tail swings outward, deforming the surface a distance ΔL to drive the leap of height H

the take-off is vertical, and provided aerodynamic losses are negligible, one may simply relate the initial kinetic energy of the body to the gravitational potential energy at the apex of the leap, mgH.

The motion of RL was characterized using high speed video (Fig. 6). The takeoff has a time scale of 3 ms, comparable to the 1 ms time for *Podura*. The leaf velocity of $U \sim 50$–100 cm/s resulted in vertical jumps of $H \sim 10$ cm, an order of magnitude larger than those of Podura owing to the relatively large elastic energy stored in the leaf spring. Characteristic parameters and dimensionless groups describing the device's motion are listed in Tables 3 and 4. As indicated by the large values of the Strouhal and Weber numbers, the dominant propulsive forces are associated with the added mass and inertia of the fluid, rather than the surface tension.

RL was able to leap consistently on the water surface, but the angle of departure of the leap was highly variable and difficult to control. It is noteworthy that its natural counterpart suffers the same problem. Smaller leapers such as *Podura* frequently tumble in the air and land on their backs. Since the leaps occur at such high speeds, both real and mechanical springtails are highly sensitive to their initial orientation.

5 Meniscus climbing

Water-walking insects at times cross from water to land in order to lay eggs and evade predators. In order to do so, they must contend with concave menisci at the borders of land that appear to them as frictionless mountains. While spiders and striders are capable of leaping over menisci, other relatively slow insects cannot and so are obliged to exploit the attraction between like-signed menisci in order to climb (Baudoin 1955). Non-wetting insects such as the water treader *Mesovelia* climb menisci by inserting retractable, hydrophilic claws into the free surface and pulling upwards (Hu and Bush 2005). The water lily leaf beetle larva *Pyrrhalta* is wetting and propels itself up the meniscus by arching its back, generating menisci at its head and tail (Fig. 7a) that are attracted to the background meniscus. This means of capillary propulsion provides the basis for the design of our mechanical meniscus climber.

In the first discussion of meniscus climbing, Baudoin (1955) demonstrated that millimetric bent metal strips ascend menisci. We have constructed a slightly more sophisticated mechanical climber (RC) five times larger than its natural counterpart, the larva *Pyrrhalta* (Fig. 7). RC consists of a rectangular plastic sheet with a thermally actuated Nitinol muscle wire stretched along its midline, attached to either end. Passing current through the muscle

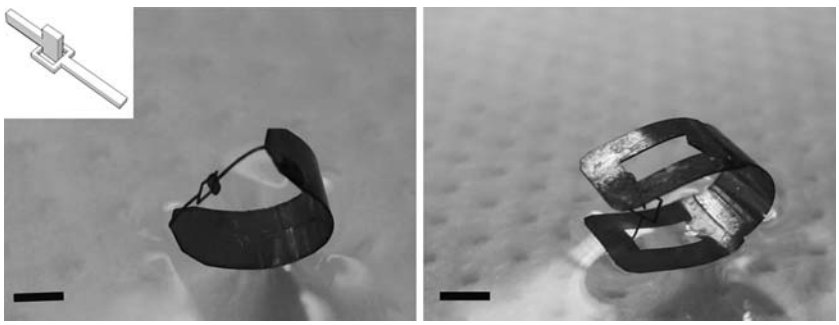

Fig. 5 Two views of the mechanical leaper floating on the water surface. The leaper is composed of a strip of metal and held in a curved posture by a micro-scale latch mechanism detailed in the *inset*. The bolt is slid into the notch; heating of the latch causes the bolt to shrink and retract from the notch. The reusable latch mechanism in the spring was cut using a pin hole steel mask (0.1 cm) and a laser (248 nm UV excimer laser from Resonetics Micromachining Systems, NH). The entire device is rendered hydrophobic with a teflon coating (static contact angle of 104°). *Scale bars* 2 mm

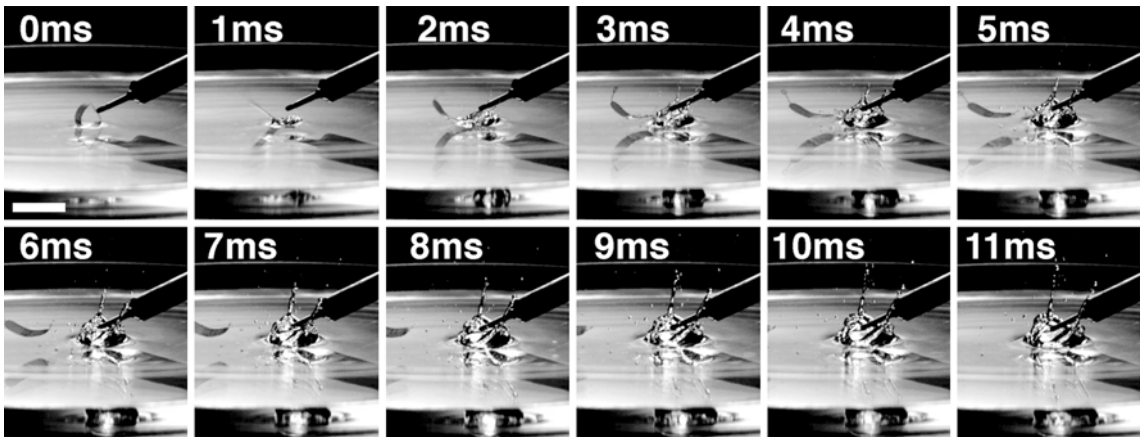

Fig. 6 High-speed video sequence of the forward jump of RL. The time-scale of the leaper's take-off is 1 ms. The mechanical leaper is actuated by heating the latch with a soldering iron (*right*) at time $t = 1$ ms. Heating releases the latch, opening the curved ends of the leaper. *Scale bar* 1 cm

Table 3 Physical parameters describing the geometry and dynamics of the mechanical leaper (RL) and its natural counterpart, the springtail *Podura aquatica*

	Body width w (cm)	Body length L (cm)	Body thickness t (cm)	Body weight Mg (dyn)	Body speed U (cm/s)	Contraction frequency f (1/s)	Body perimeter P (cm)
Springtail	0.01	0.05	0.01	0.1	50	1,000	0.1
RL	0.2	1.3	7.5×10^3	4	50–100	1,000	3

Table 4 Dimensionless groups characterizing the geometry and dynamics of the mechanical leaper (RL) and its natural counterpart

	Body aspect ratio $\lambda = \frac{w}{L}$	Reynolds $Re = \frac{Uw}{\nu}$	Bond $Bo = \frac{\rho g w^2}{\sigma}$	Weber $We = \frac{\rho U^2 w}{\sigma}$	Strouhal $St = \frac{wf}{U}$	Baudoin $Ba = \frac{\mathrm{Mg}}{\sigma P}$
Springtail	0.2	50	1.4×10^{-3}	0.4	0.2	1.2×10^{-2}
RL	0.15	10^3	0.6	7–28	2–4	1.3×10^{-2}

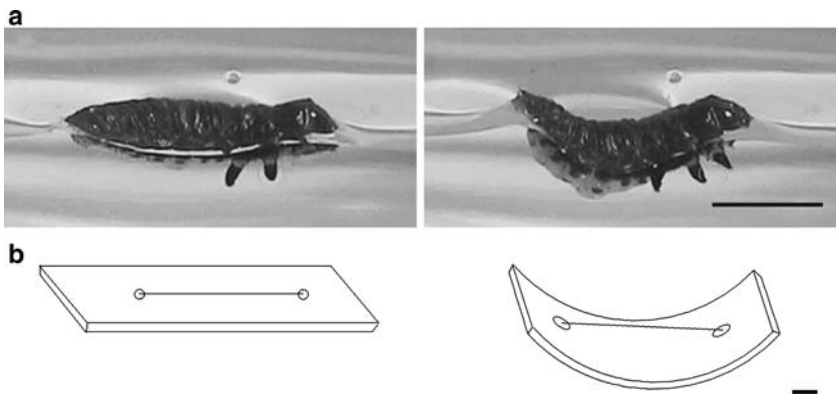

Fig. 7 Natural and mechanical mensicus climbers. **a** The beetle larva climbs the meniscus by arching its back, deforming the water surface at its head and tail. **b** For the mechanical meniscus climber, arching is prompted by the contraction of a temperature-sensitive muscle wire. *Scale bars* 3 mm

wire leads to ohmic dissipation; the resulting heating causes the wire to contract and the sheet to bend. When the wire is relaxed, the sheet's inherent stiffness provides the opposing force that returns RC to a planar state. The sheet material, lexan plastic (density 1.2 g/cm^3) was chosen so that RC would be sufficiently lightweight to be supported by surface tension. Lexan is also wetting, which allows it to deflect the free surface vertically.

The most important design parameter for RC was the size of the rectangular plastic sheet. Once the muscle wire

is contracted, a non-zero force F_{cold} is required to stretch it back to its original length. When contracting, the muscle wire exerts a maximum force F_{hot}, typically five times F_{cold} (Mondotronics, Co.). The sheet therefore must be sufficiently stiff to deform the cold relaxed wire, yet sufficiently compliant to be deformed by the hot contracted wire. This constraint may be written

$$F_{hot} > 8\frac{EI}{L^2} > F_{cold} \tag{2}$$

where E, I and L are the Young's modulus, area moment of inertia, and length of the sheet (Crandall et al. 1978). For the muscle wire used in our device, a lexan sheet with Young's modulus 2.3×10^{10} dynes/cm^2, length L, width w and thickness t listed in Table 5 was sufficient to satisfy (2).

RC is shown climbing in Fig. 8. Voltage supplied by an external power source causes RC to arch and so ascend the meniscus at an average speed of 1 cm/s. Its motion is characterized by the dimensionless groups listed in Table 6. For both RC and its natural counterpart, the dominant propulsive force is the curvature force generated by deforming the free surface.

6 Concluding remarks

We have enumerated the fundamental principles to be considered in the design of water-walking devices. Moreover, we have applied these principles in the design and construction of biomimetic mechanisms capable of rowing, leaping and meniscus climbing. We first required that our devices be sufficiently light to be supported by surface tension. This constraint was satisfied through a judicious choice of thin lightweight metals and composites. Second, we required our devices, with the exception of our mechanical meniscus climber, to be non-wetting. Our devices were made non-wetting by constructing or coating them with hydrophobic material. We also required that our devices not penetrate the surface during their driving stroke. The peak speeds and applied forces were constrained accordingly.

Much remains to be learned from water-walking arthropods. Though descended from terrestrial insects (Andersen 1982), they have since evolved several key adaptations for survival on the water surface, the most important being their water-repellency. Given the risk of entrapment by the interface, maintenance of their hydrophobicity is critical to their survival. For our mechanical water walkers, water repellency was provided by a hydrophobic coating on their legs. For water-walkers, water repellency is provided by a complex carpet of hairs; the nature of the dynamic interaction between this hair layer and the free surface is considered by Bush et al. (2007). Advances in the design and construction of water-walking devices will rely on the use of roughened hydrophobic surfaces reminiscent of insect integument, that will

Table 5 Physical parameters describing the geometry and dynamics of the mechanical climber (RC) and its natural counterpart, *Pyrrhalta*

	Body width w (cm)	Body length L (cm)	Body thickness t (cm)	Body weight Mg (dyn)	Body speed U (cm/s)	Contraction frequency f (1/s)	Body perimeter P (cm)
Beetle larva	0.3	0.6	0.3	25	10	0.3	2
RC	0.1	3.5	0.1	500	1	0.6	7

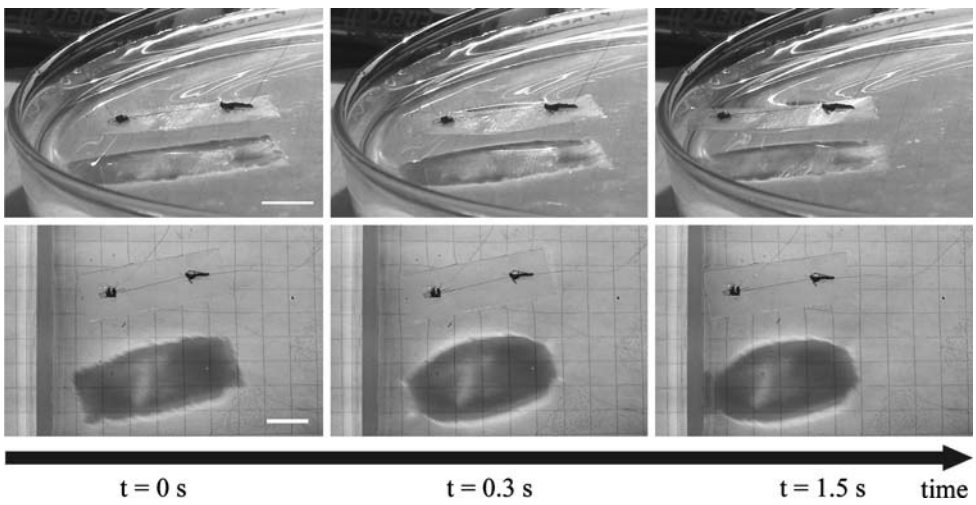

Fig. 8 Oblique views of the mechanical meniscus climber. The ascent takes roughly 1.5 s and begins when Roboclimber arches its back at $t = 0.3$ s. The deformation of the free surface due to the arching is reflected in the alteration of the underlying shadow. *Scale bars* 1 cm

Table 6 Dimensionless groups characterizing the geometry and dynamics of the mechanical climber (RC) and its natural counterpart

	Body aspect ratio $\lambda = \frac{w}{L}$	Reynolds $Re = \frac{Uw}{\nu}$	Bond $Bo = \frac{\rho g w^2}{\sigma}$	Weber $We = \frac{\rho U^2 w}{\sigma}$	Strouhal $St = wf\ U$	Baudoin $Ba = \frac{\mathrm{Mg}}{\sigma P}$
Beetle larva	0.5	300	1.3	0.4	0.01	0.3
RC	0.4	100	22	0.02	0.8	0.9

substantially alter the nature of the interaction between the device and the free surface.

The greatest difficulty in building a reliable water-walker is preventing it from breaking the free surface during its driving stroke. The designers of micromechanical walkers, swimmers and fliers have emphasized that a control system is the way most creatures tune themselves to their environments (Dickinson et al. 2000). In the case of water-walkers, a control system could be implemented to measure the force applied by the leg to the free surface. Another means of preventing the leg from penetrating the free surface would be to increase its flexibility. Recent work on compliant bodies, such as by Alben et al. 2002, may shed light on this issue.

While the precarious nature of water-walking devices raises questions as to their practicality on the open ocean, they may yet find application in laboratory settings. Enabling water-walkers to be independent, remote-controlled devices is a step recently taken by Suhr et al. (2005) and Basso et al. (2005), who have built the next generation of water-walkers to be directed by wireless remote controllers and powered by solar energy. It should also be possible to design a water-walker that can change its wetting properties on command using recent advances in smart microfluidics (e.g. Darhuber and Troian 2005).

Acknowledgments JWMB gratefully acknowledge the financial support of the NSF through Career Grant CTS-0130465; DLH likewise through an NSF Postdoctoral Fellowship. MP acknowledge financial support of NSF Grant CCR-0122419.

References

Alben S, Shelley M, Zhang J (2002) Drag reduction through self-similar bending of a flexible body. Nature 420:479–481

Andersen NM (1976) A comparative study of locomotion on the water surface in semiaquatic bugs (Insects, Hemiptera, Gerromorpha). Vidensk Meddr Dansk Naturh Foren 139:337–396

Andersen NM (1982) The semiaquatic bugs (Hemiptera, Gerromorpha): phylogeny, adaptations, biogeography and classification. Scandinavian Science Press Ltd, Klampenborg, Denmark

Basso B, Fong A, Hurst A, Knapp M (2005) Robot using surface tension (R.U.S.T.Y). Undergraduate thesis, Columbia University

Baudoin R (1955) La physico-chimie des surfaces dans la vie des Arthropodes aeriens des miroirs d'eau, des rivages marins et lacustres et de la zone intercotidale. Bull Biol Fr Belg 89:16–164

Bush JWM, Hu DL (2006) Walking on water: biolocomotion at the interface. Ann Rev Fluid Mech 38:339–369

Bush JWM, Prakash M, Hu DL (2007) The integument of water-walking arthropods: form and function. Adv Insect Physiol (in press)

Crandall SH, Dahl NC, Lardner TJ (1978) An introduction to the mechanics of solids. McGraw-Hill, Inc., New York

Darhuber AA, Troian SM (2005) Principles of microfluidic acutation by modulation of surface stresses. Annu Rev Fluid Mech 37:425–455

Dickinson MH, Lehmann FO, Sane SP (1999) Wing rotation and the aerodynamic basis of insect flight. Science 284:1954–1960

Dickinson MH, Farley CT, Full RK, Koehl MAR, Kram R, Lehman S (2000) How animals move: an integrated view. Science 288:100–106

Fearing RS, Chiang KH, Dickinson M, Pick DL, Sitti M, Yan J (2000) Wing transmission for a micromechanical flying insect. In: Proc. of IEEE Int. Conf. Robot. Auton., pp 1509–1516

Fish FE (2006) The myth and reality of Gray's paradox: implication of dolphin drag reduction for technology. Bioinsp Biomim 1:R17–R25

Floyd S, Keegan T, Palmisano J, Sitti M (2006) A novel water running robot inspired by basilisk lizards. In: Proc. of the IEEE/RSJ intl. conf. on intell. robot. and sys, pp. 5430–5436

Gao X, Jiang L (2004) Water-repellent legs of water striders. Nature 432:436

Geim AK, Dubonos SV, Grigoreiva IV, Novoselov KS, Zhukov AA, Shapoval YS (2003) Microfabricated adhesive mimicking gecko foot-hair. Nat mater 2:461–463

Glasheen JW, McMahon TA (1996a) A hydrodynamic model of locomotion in the basilisk lizard. Nature 380:340–342

Glasheen JW, McMahon TA (1996b) Size dependence of water-running ability in basilisk lizards *Basiliscus basiliscus*. J Exp Biol 199:2611–2618

Heishichiro O, Ryutaro K, Nawa Y (1966) Ninja exhbition booklet. Iga Ninja Museum, Japan

Holdgate MW (1955) The wetting of insect cuticle by water. J. Exp. Biol 591–617

Hu DL, Bush JWM (2005) Meniscus-climbing insects. Nature 437:733–736

Hu DL, Chan B, Bush JWM (2003) The hydrodynamics of water strider locomotion. Nature 424:663–666

Landau LD, Lifshitz EM (1986) Theory of elasticity, 3rd edn. Pergamon Press, New York

Leonardo da Vinci (1478–1518) Codex atlanticus. Biblioteca Ambrosiana, Milan, p 26

Li J, Hesse M, Ziegler J, Woods AW (2005) An arbitrary Lagrangian Eulerian method for moving-boundary problems and its application to jumping over water. J Comput Phys 208:289–314

Long JH, Schumacher J, Livingston N, Kemp M (2006) Four flippers or two? Tetrapodal swimming with an aquatic robot. Bioinsp Biomim 1:2029

Luo J, He JH, Flewitt A, Spearing AM, Fleck NA, Milne WI (2005) Development of all metal electrothermal actuator and its applications. J Microlith Microfab Microsyst 4(2):1–10

McMahon TA, Bonner JT (1985) On size and life. Sci. Am. Libr., New York, p 211

Ray J (1710) Historia insectorum. Impensis/Churchill, London

Shi F, Wang Z, Zhang X (2005) Combining a layer-by-layer assembling technique with electrochemical deposition of gold aggregates to mimic the legs of water striders. Adv Mater 17:1005–1009

Song YS, Suhr SH, Sitti M (2006) Modeling of the supporting legs for designing a biomimetic water strider robot. In: Proc IEEE Int Conf Robot Auton., pp 2303– 2310

Suhr SH, Song YS, Lee SJ, Sitti M (2005) A biologically inspired miniature water strider robot. In: Proc Robot Sci Sys, pp 42–48

Suter RB (2003) Trichobothrial mediation of an aquatic escape response: directional jumps by the fishing spider. J Insect Sci 3:1–7

Suter RB, Gruenwald J (2000) Predator avoidance on the water surface? Kinematics and efficacy of vertical jumping by *Dolomedes* (Araneae, Pisauridae). J Arachnol 28(2):201–210

Triantafyllou MS, Triantafyllou GS, Yue DKP (2000) Hydrodynamics of fishlike swimming. Annu Rev Fluid Mech 32:33–53

Tseng M, Rowe L (1999) Sexual dimorphism and allometry in the giant water strider *Gigantometra gigas*. Can J Zool 77:923–929

Whitesides GM, Grzybowski B (2002) Self-assembly at all scales. Science 295:2418–2421